European Society of Computational Methods in Sciences and Engineering (ESCMSE)

Journal of Numerical Analysis, Industrial and Applied Mathematics (JNAIAM)
vol. 19, no. 3-4, 2026, pp. 21-32
ISSN 1790–8140

Analysis of MHD Entropy Generation of Radiative Flow Past a Nonlinear Stretching Porous Plate

Wekesa.W. Simon, K. Hriczó[1]

Department of Analysis,
Institute of Mathematics,
Faculty of Mechanical Engineering and Informatics,
University of Miskolc,
3515 Miskolc, Hungary.

Received 7 August, 2025; accepted in revised form 31 October, 2025

Abstract:
Modern industrial applications demand robust numerical methods capable of handling large-scale, nonlinear, and diverse mathematical models. This study investigates magnetohydrodynamic entropy generation associated with the radiative flow of a nanofluid past a nonlinearly stretching porous plate. The methodology employs the Tiwari-Das two-phase model to represent the nanoparticle volume fraction and incorporates effects such as internal heat generation and thermal radiation in a porous medium. Through the application of similarity transformations, the governing partial differential equations for momentum, energy, and concentration are reduced to a system of nonlinear ordinary differential equations, which are then solved numerically using a shooting technique coupled with a Runge-Kutta algorithm implemented via the MATLAB ode45 solver. The primary findings demonstrate how variations in physical parameters, including magnetic field intensity and porosity, directly influence the flow variables and the corresponding entropy generation rates. The insight improves industrial numerical machining, analysis and optimisation of climate and environmental models, data science and machine learning, operations research, and simulation of computational fluid dynamics.

Keywords: Entropy generation, MHD flow, porous medium, similarity transformation.

Mathematics Subject Classification: 35Q30

PACS: 02.30Jr, 44.30 +v, 47.65.−d

1. Introduction

Numerical analysis plays a crucial role in solving complex models for industrial applications. The techniques apply to processes and extract information that is used for decision-making in areas such as nanofluid, finance, and quantity surveying. Computation finds solutions to a nanofluid circulating over the surface of solar collectors. The information is applied in solar dryers for the maximisation of heat absorption. The optimisation of the flow of heat in perforated metal foams heated by external radiation, like furnaces and nuclear reactors in combustion chambers and heat exchangers, is through numerical computation. With the emergence of electric vehicles such as electric trains, cars, drones, and the related machine design, optimisation requires quantitative solutions. Robotics and automation achieve efficient motion through iterations. The development and future perspective of the Tiwari and Das model in nanofluid flow for different geometries, considering viscosity and thermal conductivity, were reviewed [10]. The thermo-physical properties raised the rate of heat transfer. The features of entropy optimisation on viscous second-grade nanofluid streamed with thermal radiation using a Tiwari and Das model were studied [2]. The growth of Reynolds and Brinkman numbers hiked the entropy of the system. [9] investigated entropy analysis of MHD hybrid nanoparticles with optical homotopy, an asymptotic method (OHAM), considering viscous dissipation and thermal radiation. The magnetic parameter and the rate of entropy generation increased the velocity profile. In [8], the authors delved into modified heat and mass fluxes on thermally radiated boundary layer flow past a stretched sheet via OHAM analysis. The temperature profile shrank with the growth of Prandtl number. [4] studied irreversibility analysis in

[1] Corresponding author. E-mail: krisztian.hriczo@uni-miskolc.hu

magnetohydrodynamics flow of ternary nanofluids over an exponentially stretching sheet with variable properties using a numerical method. The results showed that the temperature profile rose with thermal conductivity. Discussing natural convection of nanofluid flow in a porous enclosure with an isothermal heated plate, the Tiwari and Das nanofluid model [5] showed that the rate of energy transfer escalates with Darcy number. The Tiwari-Das nanofluid model for magnetohydrodynamics (MHD) natural convective flow of a nanofluid adjacent to a spinning down-pointing vertical cone was examined [1]. Findings posted that the rate of heat transfer is a function of particle concentration. In [7], the authors analysed the entropy generation in natural convection of nanofluid inside a square cavity having a hot solid block: Tiwari and Das model. Convective flow inside a cavity improved the heat transfer rate. The entropy generation characteristics in the flow of nanofluids over an unsteady stretching surface under the combined effects of magnetic field and suction/injection were explored [3]. The outcome showed that the rise of the magnetic field decreased the momentum. Exploring the irreversibility process and thermal energy of a tetra hybrid radiative binary nanofluid focusing on solar implementations, the findings reported that solar radiation grew the heat in the fluid [6]. Using the similarity transformation technique, the fluid flow through porous surfaces was investigated for nanofluids and different slip conditions in [11-13]. None of the aforementioned literature discusses irregular stretching of a porous plate. This study fills the gap by considering MHD solar radiation using the Tiwari-Das model.

2. Methodology

The general equations describing the flow of a fluid with the presence of magnetic field are presented by considering electromagnetic body force per unit volume (F).

$$F = \vec{J}x\vec{B}, \tag{1}$$

with J as the electric current density and B as the magnetic field respectively. The electromagnetic power (q).

$$q = \vec{J}\,\vec{E}, \tag{2}$$

where E is the electric field. Ohm's law expresses a current density field as

$$\vec{J} = \sigma(\vec{E} + \vec{V}x\vec{B}), \tag{3}$$

By neglecting the effect of electric field, $\vec{E} = 0$, in presence of a transverse magnetic field, volumetric power dissipation is stated.

$$q_v = \frac{J^2}{\sigma}, \tag{4}$$

The vector representation of the continuity, momentum and energy is expressed as follows

$$\nabla\vec{V} = 0, \tag{5}$$

$$\rho\vec{V}(\nabla\vec{V}) = \mu(\nabla^2\vec{V}) - \vec{J}x\vec{B} - \mu(\nabla\vec{V}), \tag{6}$$

$$\vec{V}(\nabla T) = k(\nabla^2\vec{V}) + Q_r'' - \mu\vec{V}(\nabla\vec{V})^2 + \frac{\vec{J}^2}{\sigma}, \tag{7}$$

The thermally absorbing particles are noninteractive; the solution is impure, and the fluid medium lacks intermolecular spacings. The flow is 2D, steady and along the x-axis, with a streamlined boundary layer, constant density, the plate stretches non-linearly and is subjected to a radiation heat source, experiences internal and external heat generation. Heat generation, conduction, viscous dissipation, radiation and porosity, a uniform magnetic field emits energy disorder. Darcy's law is utilised for porous media. Based on the assumptions aforesaid, the following schematic geometry describes the flow regime.

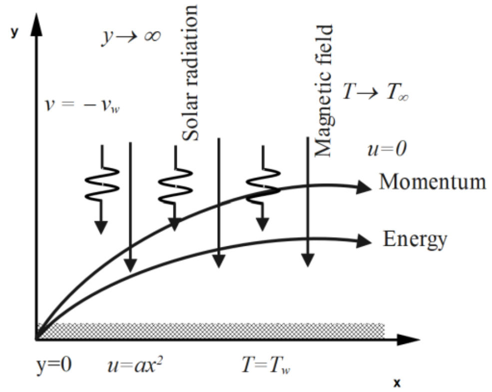

Figure 1: Schematic geometry

The effect of solar radiation is modelled as a volumetric heat source $Q_r'' = Q_o I_o e^{-\beta y}$. The symbols represent the intensity of incident radiation (Q_o), the radiation absorption coefficient (β), initial intensity (I_o), depth of penetration (y). In spatial co-ordinates, specific equations (5)-(7) are presented as follows.

$$\frac{\partial u}{\partial x} + \frac{\partial v}{\partial y} = 0, \tag{8}$$

$$u\frac{\partial u}{\partial x} + v\frac{\partial u}{\partial y} = \frac{\mu}{\rho}\frac{\partial^2 u}{\partial y^2} - \frac{\sigma\beta^2}{\rho}u - \frac{\mu u}{k}, \tag{9}$$

$$u\frac{\partial T}{\partial x} + v\frac{\partial T}{\partial y} = \alpha\frac{\partial^2 T}{\partial y^2} + Q_r'' - \frac{\mu u}{\rho C_p}\left(\frac{\partial u}{\partial y}\right)^2 + \frac{\sigma\beta_o^2}{\rho C_p}u^2, \tag{10}$$

The constraints bind the flow of the fluid past an irregularly stretching plate.
At y=0

$$u = u_w = ax^n, v_w = -v_o x^m, T = T_\omega = T_\infty + Ax^n, \tag{11}$$

Far away from the wall $y \to \infty$

$$u \to 0, T \to \infty, \tag{12}$$

The symbols represent wall velocity (u_w), wall suction (v_w), nonlinear coefficient of velocity (a), temperature at and far away from the wall (T_w, T_∞).

The similarity, dimensionless temperature, stream function, and velocity fields variables were defined as

$$\left.\begin{aligned} \eta &= \left(\frac{a(n+1)}{2\gamma}\right)^{\frac{1}{2}} x^{\frac{n-1}{2}}, T = T_\infty + \theta(T_w - T_\infty), \psi = (a\gamma)^{\frac{1}{2}} x^{\frac{n+1}{2}} f, \\ u &= \frac{\partial\psi}{\partial y} = ax^n f', v = -\frac{\partial\psi}{\partial y} = -\left(\frac{a\gamma(n+1)}{2}\right)^{\frac{1}{2}} x^{\frac{n-1}{2}}\left(\frac{n+1}{2}f - \frac{n-1}{2}\eta f'\right), \end{aligned}\right\} \tag{13}$$

The nondimensional equations (14)-(16) are obtained when equation (13) is applied into equations (8)-(10) and (11)-(12).

$$f''' + \frac{n+1}{2}ff'' - nf'^2 - Mf' - Kf' = 0, \tag{14}$$

$$\theta'' + Pr\left(\frac{n+1}{2}f\theta' - nf'\theta\right) = -S + PrEcf'' + PrM_\theta f'^2, \tag{15}$$

$$\left.\begin{array}{l} f' = 1,\ f = f_o,\ \theta = 1 \ \text{as}\ \eta = 0, \\ f' = 0,\ \theta' = 0 \ \text{as}\ \eta \to \infty, \end{array}\right\} \tag{16}$$

where Prandtl (Pr), and Eckert (Ec), magnetic parameters (M), porosity (K), radiation source (S), heat absorption coefficient (λ), Joule heating (M_θ), energy source entropy (S_o), Reynolds number (Re) and temperature ratio (ϵ) were obtained as

$$Pr = \frac{\gamma}{\alpha},\ Ec = \frac{c^2}{C_p(T_w - T_\infty)},\ M = \frac{\sigma\beta^2}{\rho c},\ K = \frac{\gamma}{ak},\ S = S_o e^{-\lambda\eta},\ \lambda = \frac{B}{\left(\frac{a(n+1)}{2\gamma}\right)^{\frac{1}{2}} x^{\frac{(n-1)}{2}}},$$
$$M_\theta = \frac{\sigma\beta_o^2}{\rho C_p},\ S_o = \frac{Q_o I_o}{\alpha(T_w - T_\infty)},\ Re_x = \frac{ax^{n-1}}{\gamma},\ \epsilon = \frac{(T_w - T_\infty)}{T_\infty},$$

3. Entropy Generation

The rate of entropy generation per unit volume (S_1) is determined using the laws of thermodynamics and non-equilibrium transport theory in watt per square meter kelvin (W/m^{2}K) as equation (17)

$$S_1 = \frac{k}{T^2}\left(\frac{\partial T}{\partial y}\right)^2 + \frac{\mu}{T}\left(\frac{\mu}{\partial y}\right)^2 + \frac{\sigma\beta^2 u^2}{T} + Q_o I_o e^{-\beta y} + \frac{\mu u^2}{KT}, \tag{17}$$

The first, second, third, fourth and fifth terms represent heat conduction, entropy absorption per unit volume, viscous dissipation, Joule heating, porous medium resistance. The characteristic entropy scale is described by equation (18).

$$S_2 = \frac{k(T_w - T_\infty)^2}{T_\infty^2 L_x^2}, \tag{18}$$

with entropy generation formulated as equation (19).

$$S_g = \frac{k}{T^2}\left(\frac{\partial T}{\partial y}\right)^2 + Q_o I_o e^{-\beta y} + \frac{\sigma\beta^2 u^2}{T}, \tag{19}$$

Applying equation (13) where $\frac{T}{T_\infty} = 1 + \theta\epsilon$, the ratio of equation (19) to (17) nondimensionalized to equation (20).

$$N_g = \frac{1}{(1+\epsilon\theta)}\left(\theta'^2 + PrEcf''^2 + PrM_\theta f'^2 + \frac{PrEc}{K}f'^2\right) + Se^{-\lambda\eta}, \tag{20}$$

In nondimensional form, the Bejan number (Be), the ratio of entropy generation to total entropy of the fluid, $Be = \frac{S_g}{S_1}$ transformed into equation (21).

$$Be = \frac{\theta'^2 + Se^{-\lambda\eta} + PrM_\theta f'^2}{\frac{1}{(1+\epsilon\theta)}\left(\theta'^2 + PrEcf''^2 + PrM_\theta f'^2 + \frac{PrEc}{K}f'^2\right) + Se^{-\lambda\eta}}, \tag{21}$$

Relative to the wall shear stress and heat flux, the skin friction and the rate of energy transfer can be determined by equation (22).

$$\left.\begin{array}{l} Cf_x = \frac{\tau_w}{\frac{1}{2}\rho u^2}, \\ Nu_x = \frac{xq_w}{k(T_w - T_\infty)}, \end{array}\right\} \tag{22}$$

with heat shear stress and heat flux as equation (23)

$$\left.\begin{array}{l} \tau_w = \mu\frac{\partial u}{\partial y}, \\ q_w = -k\frac{\partial T}{\partial y}, \end{array}\right\} \tag{23}$$

Upon substitution of equation (23), equation (22) transforms into equation (24).

$$\left.\begin{aligned} Cf_x Re_x^{\frac{1}{2}} &= \left(2(n+1)\right)^2 f'', \\ Nu_x Re_x^{-\frac{1}{2}} &= -\left(\frac{n+1}{2}\right)^{\frac{1}{2}} \theta', \end{aligned}\right\} \tag{24}$$

with local skin friction coefficient (Cf_x), local Reynolds (Re_x) and the Nusselt numbers (Nu_x) respectively.

The deployment of spatial variables converted the non-linear equations (14)-(15) into a system of first order linear equations (25)-(29)

$$y_1 = f, y_2 = f', y_3 = f'', y_4 = \theta, y_5 = \theta',$$

$$y_1' = y_2, \tag{25}$$

$$y_2' = y_3, \tag{26}$$

$$y_3' = -\frac{n+1}{2} y_1 y_2 + n y_2^2 + (M+K) y_2, \tag{27}$$

$$y_4' = y_5, \tag{28}$$

$$y_5' = -Pr\left(\frac{n+1}{2} y_1 y_5 - n y_2 y_4\right) - S - Pr\, Ec y_3 + Pr\, M_1 y_2^2, \tag{29}$$

Numerical procedure

The presence of nonlinearity terms in the system of ODEs (25)-(29) prevents the determination of the solution by analytical methods. A numerical shooting technique was employed. The unknown conditions were identified as $f''(0)$ and $\theta'(0)$ together with the initial conditions of equation (16) spatially transformed into the expression (30).

$$y_2(0) = 1, y_1(0) = f_o, y_3(0) = f''(0), y_4(0) = 1, y_5(0) = \theta'(0), \tag{30}$$

The initial values of the unknows were chosen as $a^{(0)}$ and $b^{(0)}$ with each integrated from $\eta = 0$ to η_{max}. To measure the scope of the boundary conditions satisfaction, the residuals were computed as R_1 and R_2.

$$R_1(a,b) = y_1(\eta_{max}),$$
$$R_2(a,b) = y_5(\eta_{max}).$$

The guesses were updated using Newton's iteration scheme

$$\begin{pmatrix} a \\ b \end{pmatrix}^{k+1} = \begin{pmatrix} a \\ b \end{pmatrix}^{k} + J^{-1} \begin{pmatrix} R_1 \\ R_2 \end{pmatrix},$$

where the Jacobian (J)

$$J = \begin{pmatrix} \frac{\partial R_1}{\partial a} & \frac{\partial R_1}{\partial b} \\ \frac{\partial R_2}{\partial a} & \frac{\partial R_2}{\partial b} \end{pmatrix}.$$

A convergence criterion was chosen at $R_1 = R_1 \leq 10^{-4}$ with relative tolerance of $\frac{R^{k+1} - R^k}{R^{k+1}} \leq 10^{-8}$. The numerical solution converged when maximum residual error of all the governing equations fell below $1.5x10^{-6}$. The tolerances ensured that computation halted when the relative differences between successive iterations became very small thereby assuring accuracy and stability of the solution.

4. Results and discussion

The consequences of the parameters on the flow are outlined and discussed by displaying the graphs for velocity, temperature, entropy generation, Bejan number, and the numerical tables of the physical quantities.

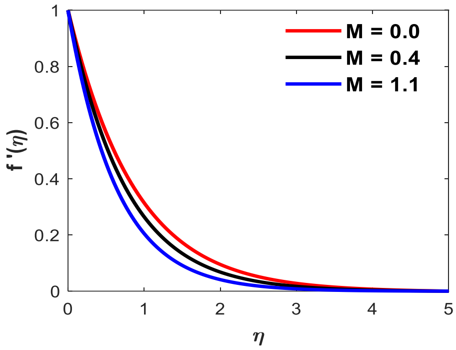

Fig.2 Effect of magnetic field on velocity.
$n = 0.5, K = 0.5, Pr = 0.72, S = 0.2, Ec = 0.01, M_\theta = 0.1, f_o = 0.2$

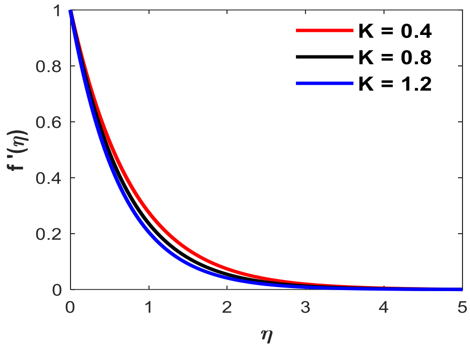

Fig.3 Effect of porosity on velocity.
$n = 0.5, S = 0.2, Ec = 0.01, \mathrm{M}_\theta = 0.1, \mathrm{f}_o = 0.2, M = 0.4, Pr = 0.72$

Figures 2-3 show the effect of magnetic field and porosity on velocity. The Lorentz force displaces the particles of the fluid. The flow of current causes a magnetic field that, in turn, resists the external force. The growth of porosity indicates the availability of more surface area and twisted flow paths of the medium to interact with the fluid. The contact raises the viscosity. Cooling gains more residential time.

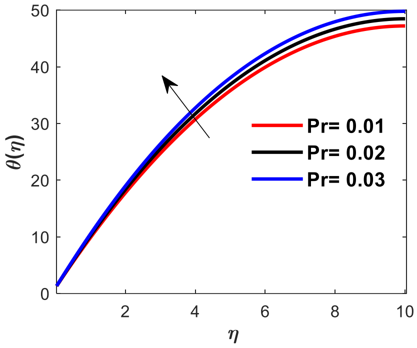

Fig.4 Effect of Prandtl number on temperature.
$n = 0.8, M_\theta = 0.1, f_o = 0.2, M = 0.2, K = 0.5, S = 0.9, Ec = 0.5$

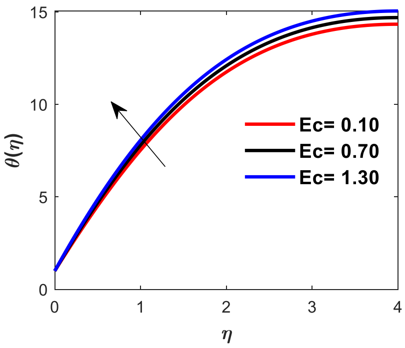

Fig.5 Effect of Eckert number temperature.
$n = 0.8, M_\theta = 0.1, f_o = 0.2, M = 0.2, K = 0.5, S = 0.9, Pr = 0.72$

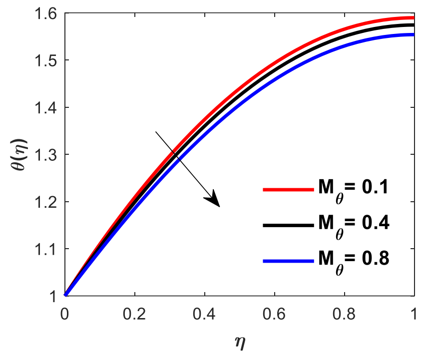

Fig.6 Effect of Joule heating on temperature.
$n = 0.8, f_o = 0.2, M = 0.2, K = 0.5, S = 0.9, Pr = 0.92, Ec = 0.5$

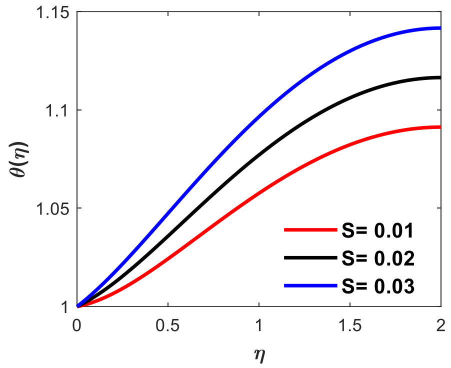

Fig.7 Effect of heat source on temperature.
$n = 0.8, M_\theta = 0.1, f_o = 0.2, M = 0.2, K = 0.5, Pr = 0.92, Ec = 0.5$

The effects of Prandtl and Eckert numbers, Joule heating and heat source are illustrated in Figs. 4-7. Fig.4 depicts the increase of Prandtl number, proportionate to viscosity, which lowers the thermal strength of the energy diffusion. The fluid layers slowly allow little heat to exit, retaining more near the surface of the wall. Momentum conduction grows more than thermal transfer. As evidenced in Fig. 5, fluid layers displace at different velocities past each other using mechanical energy (M.E). When Eckert number soars, the internal friction converts some of the M.E associated with the flow into heat. In Fig. 6, the growth of Joule heating (M_θ) negatively impacts temperature by enhancing convective cooling. The reduction in electrical resistance escalates electromagnetic dumping, which suppresses velocity. Convective transfer of heat decays. Figure 7 demonstrates the effect of solar radiation. More radiant energy adds to the fluid per unit volume. The excess heat spreads, thickening the thermal boundary layer, thus elevating the temperature.

Figures 8-11 portray the impacts of magnetic field, Joule heating, porosity, and heat source. Figure 8 shows that the magnetic field damps the motion of the fluid. Heat generation due to viscosity decreases. Figure 9 indicates a positive change in temperature with Joule heating. The resistance due to the interaction of the magnetic current and the external magnetic field converts mechanical and electrical energy, causing heated motion. The local temperature of the fluid rises. The steep difference in temperature spreads heat. Resistance irreversibly loses electrical energy. Figure 10 portrays growth in the size of the pores, allowing fluid to seep through with ease since more space is available. The fluid encounters less resistance near the wall, de-escalating viscous heating. The velocity decay and reduced drag force cause less viscosity, and so does entropy. The outcome of Fig. 11 outlines that solar radiation supplies more radiant heat. The transfer makes the thermal boundary layer energy fat, amplifying entropy.

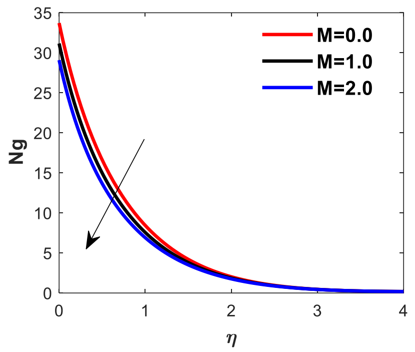

Fig.8 Effect of magnetic field on entropy.

$n = 0.4, M_\theta = 0.1, f_o = 0.2, K = 0.5, Pr = 0.92, Br = 0.4, \epsilon = 0.2, \lambda = 0.3, S = 0.6, Ec = 0.5$

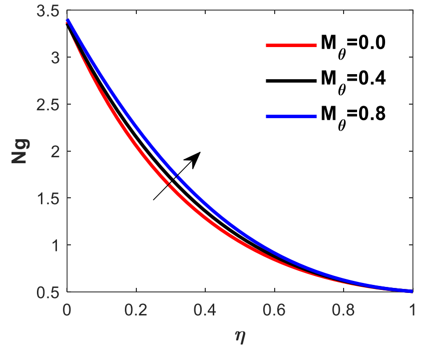

Fig.9 Effect of Joule heating on entropy.

$n = 0.6, K = 0.3, Pr = 1.92, Br = 0.1, \epsilon = 0.6, \lambda = 0.5, S = 0.8, Ec = 0.5, M = 0.2, f_o = 0.2$

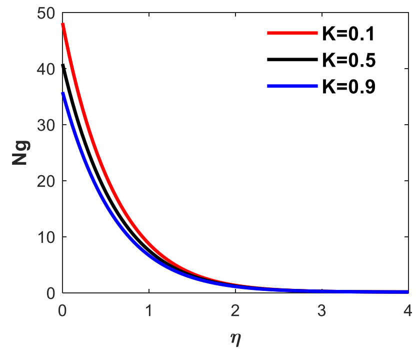

Fig.10 Effect of porosity on the entropy.

$n = 0.2, Pr = 1.62, Br = 0.1, \epsilon = 0.2, \lambda = 0.2, S = 0.3, Ec = 0.5; M = 0.2, M_\theta = 0.4, f_o = 0.2$

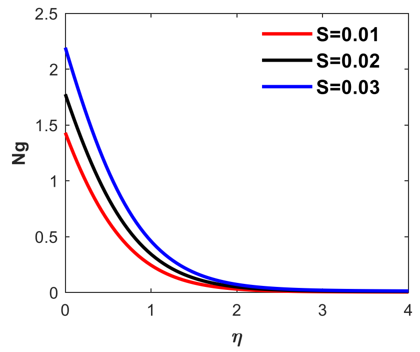

Fig.11 Effect of solar radiation on the entropy.

$n = 0.2, Pr = 1.62, Br = 0.1, \epsilon = 0.2, \lambda = 0.2, Ec = 0.5, M = 0.2, M_\theta = 0.4, f_o = 0.2K = 0.5$

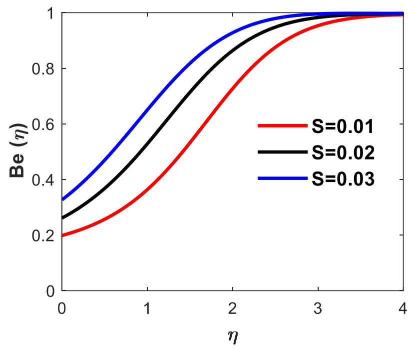

Fig.12 Effect of heat source on the Bejan number.
$n = 0.2, M = 0.2, K = 0.5, Pr = 0.4, Ec = 0.4, M_\theta = 0.1, f_o = 0.2, \lambda = 0.3, Br = 0.1, \epsilon = 0.1$

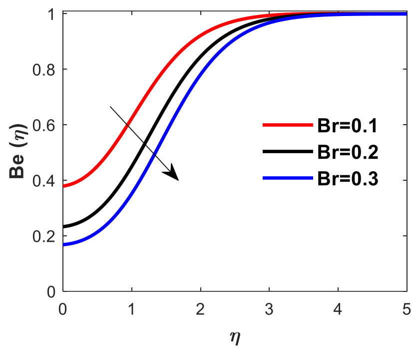

Fig.13 Effect of Brinkmann number on the Bejan number.
$n = 0.4, M = 0.3, K = 0.5, Pr = 0.62, Ec = 0.1, M_\theta = 0.3, f_o = 0.2, \lambda = 0.3, \epsilon = 0.02, S = 0.02$

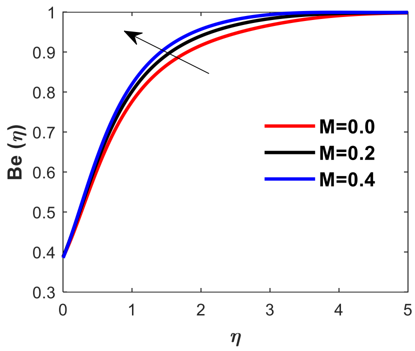

Fig.14 Effect of magnetic field on the Bejan number.
$n = 0.2, K = 0.35; Pr = 0.1, Ec = 0.15, M_\theta = 0.15, f_o = 0.2, \lambda = 0.01, S = 0.02, Br = 0.6, \epsilon = 0.2$

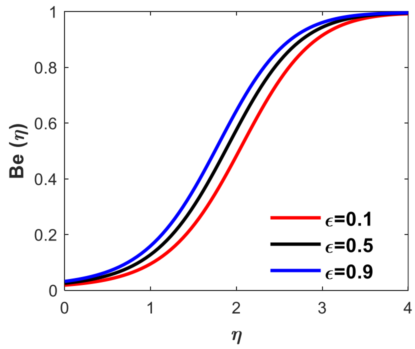

Fig.15 Effect of temperature coefficient on the Bejan number.
$n = 0.2, K = 0.35, Pr = 0.1, Ec = 0.15, M_\theta = 0.15, f_o = 0.2, \lambda = 0.01, S = 0.02, Br = 0.6, M = 0.3$

Figure 12 shows that the solar radiation increases with temperature. The irreversibility of heat transfer develops faster than the combined viscous dissipation and Joule heating. Radiation adds external heat energy to the fluid thermal boundary layer. Figure 13 reveals the progress of Brinkman number causes viscous heating. Non-reversible heat transfer increases faster than frictional heat transfer. The flow of heat, at constant temperature gradient, minimises anergy. Figure 14 conveys magnetic field grows with the irreversibility of heat transfer. While the Lorentz force reduces velocity, causing a decrease in skin friction and viscous entropy, Ohmic heating increases. Thermal energy escalates in the fluid. Figure 15 exemplifies temperature coefficient enlargement with lost energy. The rise in wall to ambient temperature difference spreads heat majorly contributing to non-reversible transport.

Table 1: Effect of porosity on skin friction and rate of energy transfer.
$(n = 0.2, M_\theta = 0.15, f_o = 0.2, Pr = 0.7, Ec = 0.15, S = 0.02)$

M	K	$Cf_x Re_x^{\frac{1}{2}}$	$Nu_x Re_x^{-\frac{1}{2}}$
0	0.1	-5.7600	0.30000
1	0.2	-7.5061	0.30014
2	0.3	-9.7092	0.30039
3	0.4	-11.487	0.30068

Table 2: Effect of nonlinearity parameter on skin friction and rate of energy transfer.
$(M_\theta = 0.15, f_o = 0.2, Pr = 0.7, Ec = 0.15, K = 0.4, S = 0.02)$

M	N	$Cf_x Re_x^{\frac{1}{2}}$	$Nu_x Re_x^{-\frac{1}{2}}$
0	0.2	-5.7600	0.3000
1	0.4	-11.388	0.3510
2	0.6	-18.780	0.40793

Table 3: Effect of solar radiation on skin friction and rate of energy transfer.
$(M_\theta = 0.15, f_o = 0.2, Pr = 0.7, Ec = 0.15, K = 0.4, n = 0.3)$

M	S	$Cf_x Re_x^{\frac{1}{2}}$	$Nu_x Re_x^{-\frac{1}{2}}$
1	0.01	-9.5792	0.32548
2	0.02	-11.804	0.32601
3	0.03	-13.661	0.32676
4	0.04	-15.288	0.32716

Table 4: Effect of Eckart number on skin friction and rate of energy transfer.
$(M_\theta = 0.15, f_o = 0.2, Pr = 0.7, K = 0.4, n = 0.3, S = 0.2)$

M	Ec.	$Cf_x Re_x^{\frac{1}{2}}$	$Nu_x Re_x^{-\frac{1}{2}}$
0.1	0.02	-6.9683	78.6620
0.2	0.04	-7.3064	35.6050
0.3	0.06	-7.6290	18.8870
0.4	0.08	-7.9381	7.41260

Table 5: Effect of Prandtl number on skin friction and rate of energy transfer.
$(M_\theta = 0.15, f_o = 0.2, Ec = 0.15, K = 0.4, n = 0.3, S = 0.2)$

M	Pr.	$Cf_x Re_x^{\frac{1}{2}}$	$Nu_x Re_x^{-\frac{1}{2}}$
0.1	2	-6.9683	49.3110
0.2	4	-7.3064	26.2060
0.3	6	-7.6290	-10.6210
0.4	8	-7.9381	-0.05782

Table 1-4 describes the effect of the rise of the magnetic field with porosity, nonlinearity, heat source, and Eckert number, all of which consequently thicken the skin friction as they increase the rate of energy transfer. Table 5 indicates that magnetic and Prandtl numbers dwindle both the skin friction and the rate of energy transfer. The higher viscosity limits diffusion of heat and momentum transfer near the wall. A larger Prandtl number inhibits thermal migration in the fluid medium. As a result, both skin friction and thermal migration lessen.

5. Conclusion

A numerical study was performed on MHD entropy generation of a radiative flow past a nonlinear steady stretching porous plate. The effects of the parameters on the flow variables, entropy, the measure of irreversibility, shear stress and the rate of energy transfer were presented and discussed. The governing equations were nonlinearized and transformed in to a first-order system through the space variables. A shooting technique, together with the Runge-Kutta method, called in MATLAB ode45, generated the graphs and tabulated numerical values. The following insights were underscored.

i. The growth of magnetic strength and porosity lower velocity.
ii. Prandtl, Eckert number and heat source raise the temperature as Joule heating reduces it.
iii. While magnetic strength and porosity decays entropy, Joule heating and heat sources improve it.
iv. Heat source, magnetic strength, and the coefficient of temperature raise the Bejan number as Brinkman number shrinks it.
v. Magnetic field strength, porosity, nonlinearity, heat source, and Eckert number decrease thermal shear stress hiking the rate of heat transfer.
vi. Combined magnetic strength and Prandtl number decreases thermal shear stress and the rate of heat transfer.

The spread of heat in a system is minimised by increasing porosity and the strength of the applied magnetic field while keeping the heat source and Joule heating low. The analysis gives insights for optimisation of efficiency with the least energy loss, control of heated flows, and for engineers to design better thermal reacting surfaces and thermal systems. Application is not limited to the field of chemical processing, the manufacture of metals and drugs.

Acknowledgement

I acknowledge the Tempus Public Foundation, the University of Miskolc and the Faculty of Mechanical Engineering and Informatics for granting me the Stipendium Hungaricum Scholarship and admission. Through the Institute of Mathematics, I thank Dr. Krisztián Hriczó, for funding the publication of this study, insightful guidance, and his prowess in the field of fluid mechanics.

References

[1] Aghamajidi, M., Yazdi, M. E., Dinarvand, S., & Pop, I. (2018). Tiwari-Das nanofluid model for magnetohydrodynamics (MHD) natural-convective flow of a nanofluid adjacent to a spinning down-pointing vertical cone. *Propulsion and Power Research*, *7*(1), 78–90. https://doi.org/10.1016/J.JPPR.2018.02.002

[2] Jamshed, W., Mishra, S. R., Pattnaik, P. K., Nisar, K. S., Suriya Uma Devi, S., Prakash, M., Shahzad, F., Hussain, M., & Vijayakumar, V. (2021b). Features of entropy optimization on viscous second grade nanofluid streamed with thermal radiation: A Tiwari and Das model. *Case Studies in Thermal Engineering*, *27*, 101291. https://doi.org/10.1016/J.CSITE.2021.101291

[3] Jarwal, V. K., Choudhary, S., Sharma, K., & Choudhary, P. (2025). Modeling and analysis of entropy in MHD unsteady flow of water-based nanofluids with carbon nanoparticles. *Discover Applied Sciences*, *7*(7). https://doi.org/10.1007/s42452-025-07256-y

[4] Kandukoori, R. C., & Janapatla, P. (2025). Irreversibility Analysis in Magnetohydrodynamics Flow of Ternary Nanofluids Over an Exponentially Stretching Sheet with Variable Properties Using Numerical Method. *Arabian Journal for Science and Engineering*. https://doi.org/10.1007/s13369-025-10356-x

[5] Lakshmi, C. V., Sireesha, M., Venkatadri, K., Fazuruddin, S., & Arigela, S. (2025b). Natural convection of nanofluid flow in a porous enclosure with isothermal heated plate: A Tiwari and Das

nanofluid model. *International Journal of Thermofluids*, *27*(May), 101238. https://doi.org/10.1016/j.ijft.2025.101238

[6] Sajid, T., Algarni, S., Ahmad, H., Alqahtani, T., Jamshed, W., Eid, M. R., Irshad, K., & Amjad, A. (2024). Exploration of irreversibility process and thermal energy of a tetra hybrid radiative binary nanofluid focusing on solar implementations. *Nanotechnology Reviews*, *13*(1). https://doi.org/10.1515/ntrev-2024-0040

[7] Sheremet, M. A., Oztop, H. F., Pop, I., Abu-Hamdeh, N., Lorenzini, G., & Mahian, O. (n.d.). *Analysis of Entropy Generation in Natural Convection of Nanofluid inside a Square Cavity Having Hot Solid Block: Tiwari and Das' Model*. https://doi.org/10.3390/e18010009

[8] Sohail, M., Rafique, E., Singh, A., & Tulu, A. (2024). Engagement of modified heat and mass fluxes on thermally radiated boundary layer flow past over a stretched sheet via OHAM analysis. *Discover Applied Sciences*, *6*(5). https://doi.org/10.1007/s42452-024-05833-1

[9] Waseem, F., Sohail, M., Ilyas, N., Awwad, E. M., Sharaf, M., Khan, M. J., & Tulu, A. (2024). Entropy analysis of MHD hybrid nanoparticles with OHAM considering viscous dissipation and thermal radiation. *Scientific Reports*, *14*(1), 1–18. https://doi.org/10.1038/s41598-023-50865-z

[10] Zafar, M., Sakidin, H., Sheremet, M., Dzulkarnain, I. B., Hussain, A., Nazar, R., Khan, J. A., Irfan, M., Said, Z., Afzal, F., & Al-Yaari, A. (2023). Recent Development and Future Prospective of Tiwari and Das Mathematical Model in Nanofluid Flow for Different Geometries: A Review. *Processes*, *11*(3). https://doi.org/10.3390/pr11030834

[11] Mahabaleshwar, U. S., Kumar, P. V., Nagaraju, K. R., Bognár, G., & Nayakar, S. R. (2019). A new exact solution for the flow of a fluid through porous media for a variety of boundary conditions. *Fluids*, *4*(3), 125. https://doi.org/10.3390/fluids4030125

[12] Jawad, M., Majeed, A., Abdelfattah, W., Bognár, G., Kamangar, S., & Hendy, A. S. (2025). Dynamics of activation energy and gyrotactic microorganisms on radiative Williamson nanofluid with Soret and Dufour bounded by porous nonlinearly stretching surface. *Journal of Radiation Research and Applied Sciences*, *18*(3), 101595. https://doi.org/10.1016/j.jrras.2025.101595

[13] Maranna, T., Mahabaleshwar, U. S., Bognar, G. V., & Oztop, H. F. (2024). Effect of radiation and injection on a Newtonian fluid flow due to porous shrinking sheet with Brinkman model. Journal of Porous Media, 27(1). https://doi.org/10.1615/JPorMedia.2023046723